Micelles Formed by a Model Hydrogen-Bonding Block Copolymer

J. Q. Zhao, E. M. Pearce,* T. K. Kwei, H. S. Jeon, P. K. Kesani, and N. P. Balsara*

Departments of Chemistry and Chemical Engineering, Polytechnic University, Six Metrotech Center, Brooklyn, New York 11201

Received October 21, 1994; Revised Manuscript Received January 5, 1995®

ABSTRACT: A nearly monodisperse polystyrene-*block*-poly(*p*-hydroxystyrene) copolymer (PS−PSOH) was synthesized by combining protected group chemistry with high-vacuum anionic polymerization. The molecular weight of both blocks was 1.0×10^4. Our objective was to study the effect of hydrogen bonding on micelle formation in block copolymer solutions. The self-hydrogen-bonding capability of the hydroxystyrene moieties is well established. Light scattering experiments were conducted on dilute solutions of PS−PSOH in tetrahydrofuran (THF), a common solvent for both blocks, and toluene, a selective solvent for the polystyrene block. Dynamic light scattering (DLS) measurements indicated that the block copolymer was molecularly dispersed (or nearly so) in THF with a hydrodynamic radius $R_h = 3.8$ nm. However, large aggregates with $R_h = 76$ nm were observed by DLS in toluene solutions. Static light scattering (SLS) measurements on the PS−PSOH/toluene solutions confirmed the presence of large aggregates with aggregation numbers of 10^4 chains/micelle. The micellar structure was determined by enforcing simultaneous consistency with both SLS and DLS measurements. A rodlike structure, 300 nm in length and 40 nm in diameter, is consistent with both measurements.

Introduction

There is continuing interest in the thermodynamic properties of block copolymers.[1,2] These macromolecules, which comprise two or more covalently bonded sequences of chemically distinct monomers, self-assemble into well-defined microstructures, both in bulk and in solution. Diblock copolymers form spherical micelles in dilute solutions if the solvent is selective, i.e., a good solvent for one block but poor for the other.[3] The micelles represent a minimum free energy structure[4] with a solvent-lean core of poorly solvated blocks and a corona of well-solvated blocks extending into solution, as depicted in Figure 1. In this respect block copolymers are similar to other amphiphilic molecules such as surfactants and phospholipids. A variety of lamellar and cylindrical structures have been identified in such systems.[5−7] Cylindrical micelles can be either rodlike or disklike, as depicted in Figure 1.

Previous studies on block copolymer micelles are largely restricted to systems wherein the inter- and intramolecular potentials are nonspecific and dominated by dispersion forces.[8] Polystyrene−polyisoprene block copolymers in hydrocarbon solvents are typical materials used in such studies.[3] The driving force for micellization in such systems is the repulsive interactions between one of the blocks and the solvent. Micelles formed under such circumstances are usually spherical,[3] although cylindrical micelles are sometimes obtained.[9,10] Recently Eisenberg and co-workers have examined micellization of ion-containing block copolymers in nonionic solvents such as toluene.[11−13] These molecules are high molecular weight analogues of traditional surfactants. In this case, the tendency for micellization is augmented by ion pair associations that can occur in the core of these micelles. Like typical nonionic block copolymers, these systems also form spherical micelles.

In this paper we report on the characteristics of micelles formed by a polystyrene-*block*-poly(*p*-hydroxystyrene) (PS−PSOH) copolymer in toluene, a selective solvent for the polystyrene block. The hydroxystyrene moieties are capable of specific interactions via hydrogen-bonding. The formation of *hydrogen bonds* in the micellar core is an additional driving force that is expected to affect micelle formation and is the distinguishing feature of this investigation. Hydrogen bonding plays an important role in both natural[14] and synthetic[15,16] polymer materials. The PS−PSOH block copolymer used in this study was synthesized by combining protected group chemistry with high-vacuum anionic polymerization.[17] Consequently, it was nearly monodisperse with respect to molecular weight and composition. The structure of the micelles was determined from static and dynamic light scattering experiments. Cylindrical micelles with a diameter of 30−40 nm and a length of about 300 nm were found to be consistent with both measurements.

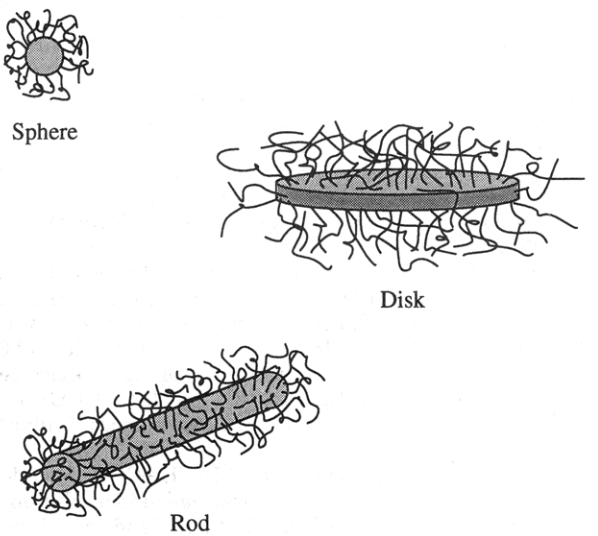

Figure 1. Schematics of possible structures of micelles in a selective solvent.

Synthesis of Polystyrene-*block*-poly(*p*-hydroxystyrene)

The reaction scheme employed for the synthesis of the polystyrene-*block*-poly(*p*-hydroxystyrene) copolymer is summarized in Scheme 1.

* Authors to whom correspondence should be addressed.

® Abstract published in *Advance ACS Abstracts,* February 15, 1995.

0024-9297/95/2228-1972$09.00/0

Scheme 1

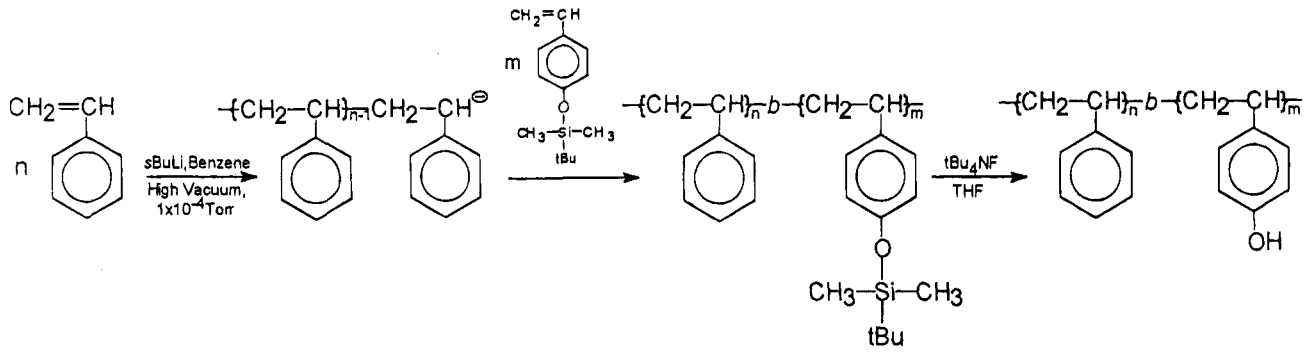

Step 1. Synthesis and Purification of *p*-[(*tert*-butyldimethylsilyl)oxy]styrene Monomer. *p*-Acetoxystyrene (64.8 g, 0.4 mol) was mixed with 10% KOH(aq) (560 mL, 1.0 mol) at 0 °C under an atmosphere of nitrogen and stirred for 2 h, followed by neutralization of the solution to a value of pH 8. Hexane was then added to extract *p*-hydroxystyrene from the solution, and the organic mixture was dried over $MgSO_4$. After filtration, hexane was evaporated to obtain a white solid. The solid was recrystallized from hexane to yield *p*-hydroxystyrene (34.7 g, yield 72%).

Mp: 68–70 °C. ^{1}H NMR (200 MHz, acetone-d_6, TMS as standard): δ 5.02–5.65 (2d, 2H, CH_2=), 6.73–6.58 (2d, 1H, CH=), 6.71–7.33 (2d, 4H, aryl–H), 8.45 (s, 1H, OH). IR: 3400 cm^{-1} (vs, OH).

tert-Butyldimethylsilyl chloride (48.2 g, 0.32 mol) in dry DMF was added dropwise into a stirred solution of *p*-hydroxystyrene (34.5 g, 0.29 mol) and imidazole (23.6 g, 0.35 mol) in dry DMF at 0 °C under an atmosphere of nitrogen. After addition was complete, the solution was allowed to warm up to room temperature and stirred for 5 h. The product was extracted using chloroform and H_2O, washed with 5% $NaHCO_3$, and dried over $MgSO_4$. After filtration and evaporation, a pale yellow liquid (63.1 g, yield 91%) was obtained.

^{1}H NMR (200 MHz, $CDCl_3$, $SiCH_3$ signal as standard): δ 0.00 (s, 6H, $SiCH_3$), 0.08 (s, 9H, $SiCCH_3$), 4.88–5.45 (2d, 2H, CH_2=), 6.37–6.54 (2d, 1H, CH=), 6.55–7.10 (2d, 4H, aryl–H). IR: 1280–1240 cm^{-1} (vs, $SiCH_3$). GC: mass = 234.

The crude product was distilled at 85 °C on a high vacuum line (10^{-4} Torr) into an evacuated ampule equipped with a break-seal. Prior to polymerization, *p*-[(*tert*-butyldimethylsilyl)oxy]styrene was further purified under high vacuum, over benzylmagnesium chloride (the mixture was stirred at room temperature for 2 h), and then distilled into another ampule with a break-seal. The purified *p*-[(*tert*-butyldimethylsilyl)oxy]styrene was colorless.

Step 2. Synthesis of Polystyrene-*block*-poly[*p*-[(*tert*-dimethylsilyl)oxy]styrene] Block Copolymer. A polystyrene-*block*-poly[*p*-[(*tert*-butyldimethylsilyl)oxy]styrene] diblock copolymer was synthesized by sequential anionic polymerization under high vacuum in benzene, with *sec*-butyllithium as the initiator and degassed isopropyl alcohol as the terminator. The polystyrene block was synthesized first. After 12 h, an aliquot of the reaction mixture containing the "living" poly(styryllithium) anions was isolated and terminated. The *p*-[(*tert*-butyldimethylsilyl)oxy]styrene monomer was then introduced into the reactor. This resulted in a change of color from bright yellow to orange. The reaction was terminated by degassed isopropyl alcohol after 4 h, at which point the orange color disappeared instantly. All the operations were carried out at room temperature, in a single, all-glass, sealed apparatus under high vacuum. Appropriate amounts of the purified reagents were attached via break-seals to the reactor. Standard high-vacuum procedures were used for purification of benzene, styrene, *sec*-butyllithium, and isopropyl alcohol.[18]

Step 3. Desilylation of Polystyrene-*block*-poly[*p*-[(*tert*-butyldimethylsilyl)oxy]styrene]. The poly[*p*-[(*tert*-butyldimethylsilyl)oxy]styrene] block was converted to poly(*p*-hydroxystyrene) by reaction with *tert*-butylammonium fluoride. The silyloxy-containing copolymer was first dissolved in THF, and a 2 M *tert*-butylammonium fluoride/THF solution was added. The mixture was stirred at room temperature under an atmosphere of nitrogen for 5 h. The polymer was precipitated by pouring the mixture into H_2O. The product was washed with H_2O, redissolved in THF, and reprecipitated by hexane.

Our synthesis procedure is based on the pioneering works of Hirao, Nakahama, and co-workers.[17]

Characterization of Polystyrene-*block*-poly(*p*-hydroxystyrene)

The chemical composition of the silyloxy-containing block copolymer was verified by ^{1}H NMR spectroscopy: ^{1}H NMR (Figure 2a) ($CDCl_3$) [(0.1 ($SiCH_3$), 0.9 ($SiCCH_3$), 1.0–2.0 (CH and CH_2), 6.1–7.2 (ArH)]. The ^{1}H NMR spectrum obtained after desilylation of the block copolymer with *tert*-butylammonium fluoride is shown in Figure 2b. The spectrum of the desilylated block copolymer is essentially devoid of peaks corresponding to the dimethylsilyl group at 0.1 ppm and *tert*-butylsilyl at 0.9 ppm (<0.5% of the protecting group is left). Instead, a peak at 9.0 ppm, corresponding to the OH group is, obtained after desilylation. The IR spectra from the silyloxy-containing block copolymer and the desilylated product are shown in Figure 3. The peak at 910 cm^{-1} obtained from the silyloxy-containing block copolymer corresponds to the Si–O bond. The spectrum from the desilylated block copolymer does not show this feature. Instead, a peak at 3450 cm^{-1} is observed, indicating the presence of the OH group.

The molecular weight of the styrene block was determined by gel permeation chromatography (GPC) on the polystyrene precursor. THF was the mobile phase, and the GPC was calibrated using polystyrene standards. The M_w of the polystyrene precursor was determined to be 1.0×10^4. The composition of the block copolymer was determined from the relative intensities of the aliphatic and aromatic protons in the ^{1}H NMR spectrum of the polystyrene-*b*-poly[*p*-[(*tert*-butyldimethylsilyl)oxy]-styrene] copolymer (Figure 2a). The M_w of the poly[*p*-[(*tert*-butyldimethylsilyl)oxy]styrene] block was determined to be 2.0×10^4. The GPC trace obtained from the block copolymer before desilylation is shown in

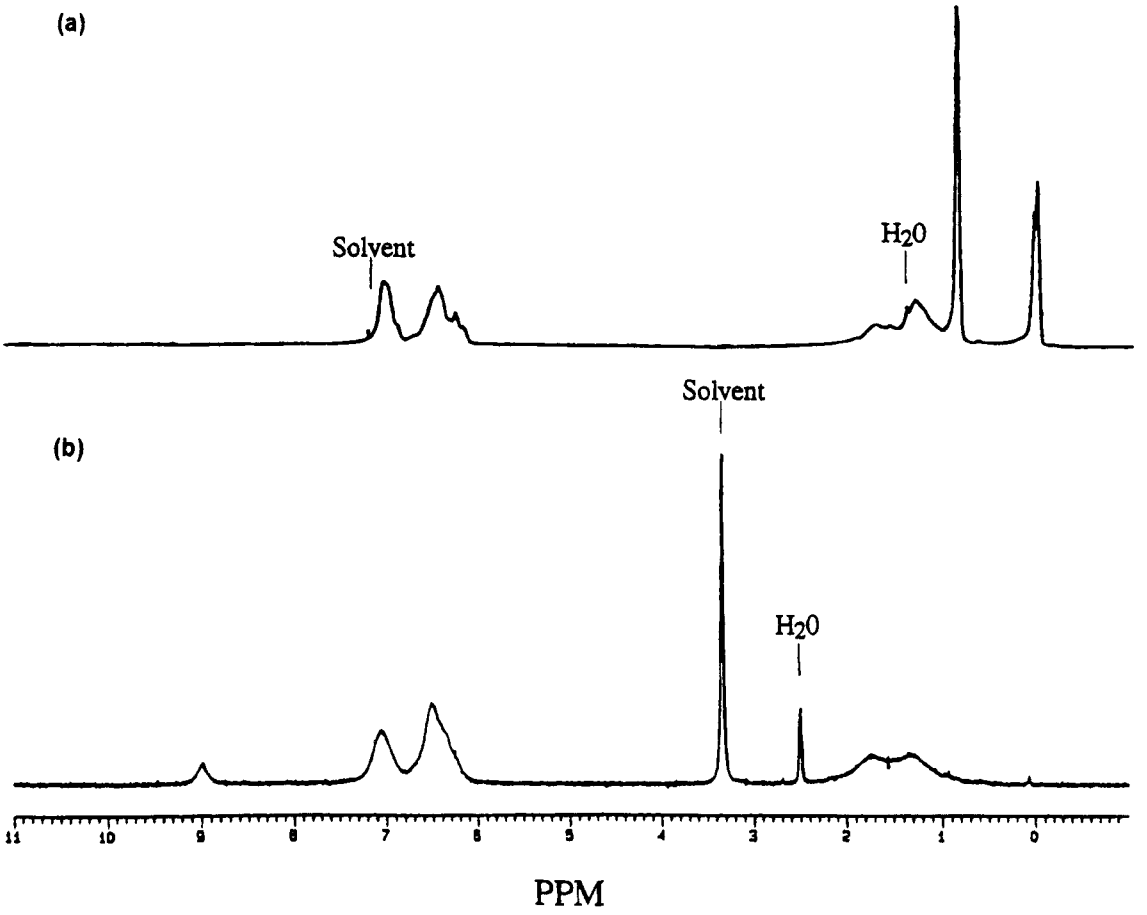

Figure 2. ^{1}H NMR spectra of (a) polystyrene-*b*-poly[*p*-[(*tert*-butyldimethylsilyl)oxy]styrene] and (b) polystyrene-*b*-poly(*p*-hydroxystyrene) copolymers.

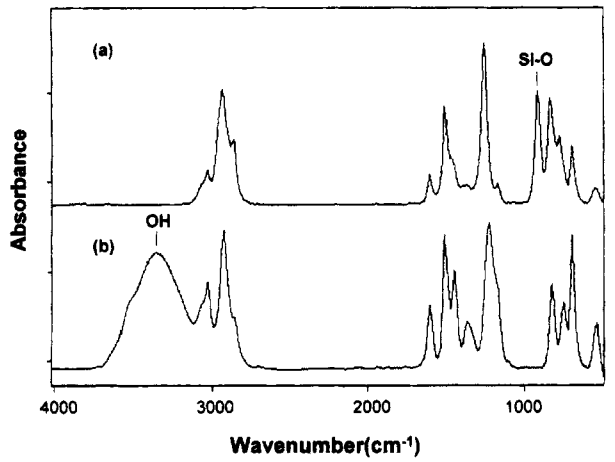

Figure 3. IR spectra of (a) polystyrene-*b*-poly[*p*[(*tert*-butyldimethylsilyl)oxy]styrene] and (b) polystyrene-*b*-poly(*p*-hydroxystyrene) copolymers.

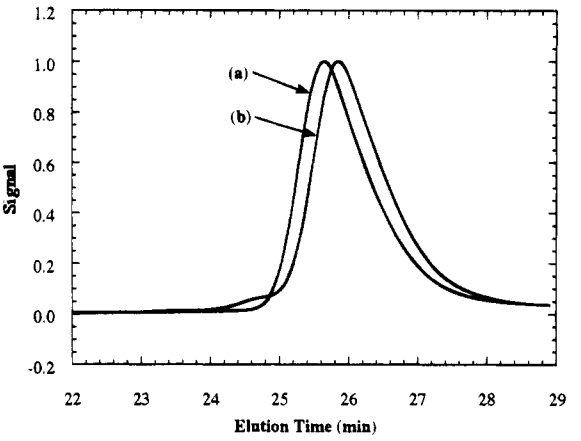

Figure 4. Gel permeation chromatograms of (a) polystyrene-*b*-poly[*p*-[(*tert*-butyldimethylsilyl)oxy]styrene] and (b) polystyrene-*b*-poly(*p*-hydroxystyrene) copolymers.

Figure 4. A single peak was obtained from the silyloxy-containing block copolymer. The polydispersity index (M_w/M_n) of this copolymer was estimated to be 1.18 based on the polystyrene calibration. The calculated molecular weight of the poly(*p*-hydroxystyrene) block after desilylation is $M_n = 1.0 \times 10^4$. The GPC data obtained from the PS–PSOH block copolymer after desilylation are also shown in Figure 4. Pyridine was added to the polymer solution prior to injection, to minimize specific interactions between the hydroxyl groups on the polymer and the stationary phase. It is likely that the "high molecular weight shoulder" that accounts for 2% of the GPC signal is due to our inability to screen the polymer–stationary phase interactions completely. Measurements without pyridine showed a shoulder of considerable height (acounting for 20% of the signal), which decreased systematically with increasing pyridine content. It is also possible that the shoulder is also due to some inter chain hydrogen bonding. Evidence for this was found in light scattering results described below.

Static and Dynamic Light Scattering Results

Static and dynamic light scattering (SLS and DLS, respectively) data from toluene and tetrahydrofuran (THF) solutions of PS–PSOH were obtained on an ALV-5000 instrument at Polytechnic University. An argon ion laser (λ = 488.0 nm) and a HeNe laser (λ = 632.8 nm) were used as sources for the incident light. Data were obtained at several scattering angles between 30 and 150°.

The SLS signals were converted to absolute intensities using pure toluene as a secondary standard. The absolute calibration was verified by measuring Rayleigh ratios of other solvents such as cyclohexane. The angular independence of the measured scattering from these low molecular weight solvents was also used to verify alignment of the instrument.

The time autocorrelation function of the scattered intensity, $g(\tau)$, was accumulated in the homodyne mode and used to obtain the intensity-weighted distribution of mobilities, $G(\Gamma)$, by solving the following integral equation.[19,20]

$$g(\tau) = B[\alpha\{\int_0^\infty G(\Gamma)\exp(-\Gamma\tau)\,d\Gamma\}^2 + 1] \qquad (1)$$

The solution was obtained using CONTIN, a software package developed by Provencher.[21]

Samples were made by encasing predetermined amounts of polymer and filtered solvents in heat-sealed glass cuvettes. Most of the samples were made using freshly opened, HPLC-grade toluene and anhydrous THF bottles, to minimize atmospheric contamination. A few THF samples were also made under high vacuum, to ensure the absence of water. Anhydrous THF was vacuum distilled, first into calcium hydride, then into a sodium dispersion, and finally into a 1:1 molar ratio of sodium and benzophenone. Scattering cells containing predetermined amounts of PS–PSOH were attached to the vacuum line by glass-blowing, and purified THF (from the THF–sodium benzophenone flask) was distilled into the cells. The scattering cells were isolated by heat-sealing. Vacuum-line integrity was maintained during all stages of sample preparation.

Toluene samples were routinely annealed at 60 °C for 48 h and then cooled to room temperature. The light scattering signals obtained from these solutions, at room temperature, a few hours after annealing, were identical to those obtained after 6 months. The exact annealing history did not appear to be important. Varying the annealing temperature from 50 to 80 °C and the annealing time from 5 to 48 h had no effect on the light scattering results. We also made a few PS–PSOH/benzene solutions, and the light scattering results were nearly identical to those obtained from the PS–PSOH/toluene solutions. The lack of time and thermal history dependence is a necessary, but not sufficient, condition for equilibrium. Thus, whether or not the imposed thermal history leads to an equilibrium state at room temperature remains an open question. We can only state that heating the samples to 50 °C or higher leads to a reproducible state at room temperature. The THF solutions were not annealed. The static and dynamic light scattering measurements reported in this paper were made on the same samples, at 25 ± 0.2 °C.

In Figure 5 we compare DLS signals obtained from typical THF and toluene solutions of PS–PSOH. Both autocorrelation functions were measured at a scattering angle of 110° [$q = 2.96 \times 10^{-2}$ nm^{-1} in THF and $q = 3.15 \times 10^{-2}$ nm^{-1} in toluene; $q = 4\pi n \sin(\theta/2)/\lambda$, where θ is the scattering angle, n is the refractive index of the solution, and λ is the wavelength of the incident beam]. The distribution of mobilities obtained from CONTIN also is shown in Figure 5. A single peak dominates this distribution in both solutions. The characteristic decay rate associated with a relaxation mode, Γ_c, is assumed to be equal to the ratio of the first and zeroth moments of the peak.

In Figure 6a we show the dependence of Γ_c of the THF solutions on q and the polymer weight fraction in

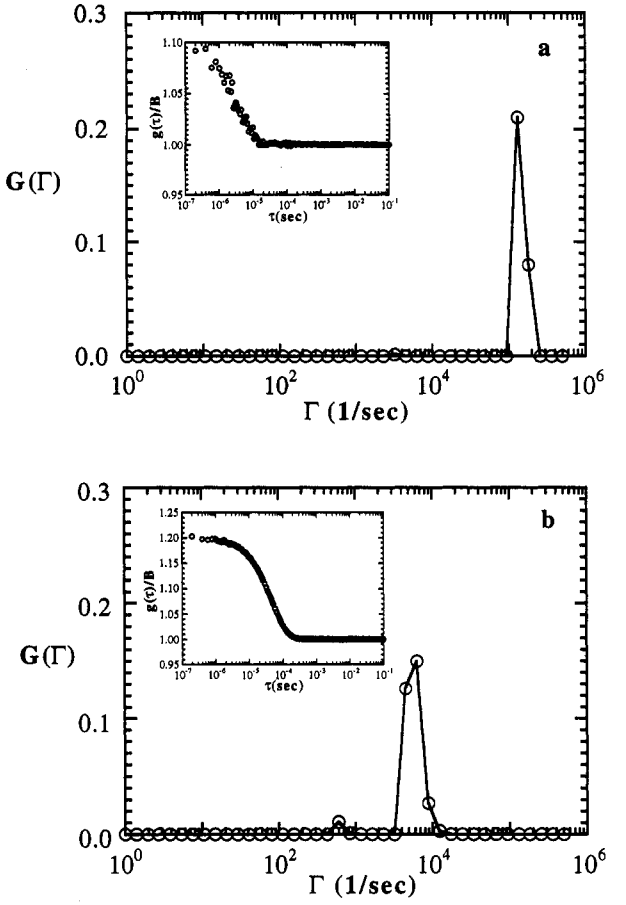

Figure 5. CONTIN results for the distribution of mobilities, $G(\Gamma)$, obtained from (a) THF ($w = 1.3 \times 10^{-2}$) and (b) toluene ($w = 3.7 \times 10^{-4}$) solutions of PS–PSOH at a scattering angle of 110°. Insets: Normalized autocorrelation functions, $g(\tau)/B$, obtained from (a) THF ($w = 1.3 \times 10^{-2}$) and (b) toluene ($w = 3.7 \times 10^{-4}$) solutions of PS–PSOH at a scattering angle of 110°.

solution, w. We have included data obtained from one of the PS–PSOH/THF samples that was prepared under high vacuum. The data obtained from this sample are identical to those obtained from solutions made under atmospheric conditions. The relaxation mode is diffusive ($\Gamma_c \sim q^2$), and the value of Γ_c at a given q is nearly independent of polymer concentration (within experimental error). The diffusion coefficient associated with this relaxation mode, D, is given by the slope of the Γ_c versus q^2 plot and is equal to 1.24×10^{-6} cm^2/s. The Stokes–Einstein relationship can be used to estimate the hydrodynamic radius of the diffusing species, R_h.

$$D = kT/6\pi\eta R_h \qquad (2)$$

where k is the Boltzmann constant, T is the absolute temperature, and η is the viscosity of the solvent. The value of R_h for PS–PSOH in THF thus obtained is 3.8 ± 0.6 nm. According to Huber et al.,[22] R_h of a 20K PS in a good solvent—in their case, toluene—is 3.3 nm. The measured R_h from the PS–PSOH/THF solutions are thus within experimental error of that expected from individual chains of the block copolymer in a good solvent. We thus conclude that the PS–PSOH is molecularly dispersed in THF. This is expected because THF is a good solvent for both PS and PSOH.

The data shown in Figure 6a were obtained several months after the samples were made. Initial DLS data from the PS–PSOH/THF solutions (obtained from samples that were prepared a week earlier) revealed a slow mode at all scattering angles, and these data were

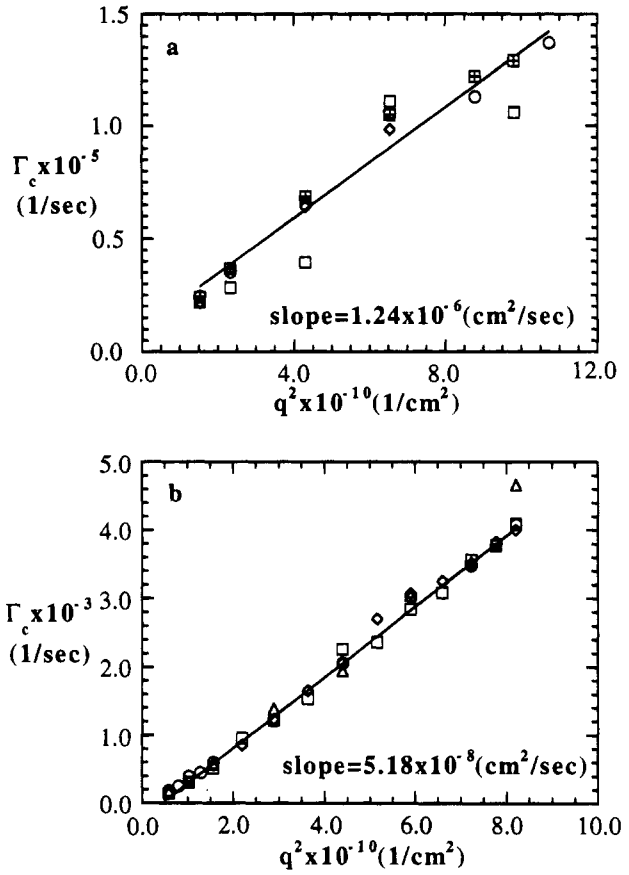

Figure 6. (a) Plot of Γ_c versus q^2 for PS–PSOH/THF solutions of various concentrations [squares, $w = 2.0 \times 10^{-3}$; circles, $w = 4.0 \times 10^{-3}$; hatched squares, $w = 1.3 \times 10^{-2}$; diamonds, sample prepared under high vacuum, $w = 1.62 \times 10^{-2}$]. (b) Plot of Γ_c versus q^2 for PS–PSOH/toluene solutions of various concentrations [triangles, $w = 6.0 \times 10^{-5}$; squares, $w = 3.0 \times 10^{-5}$; diamonds, $w = 1.5 \times 10^{-4}$; circles, $w = 3.7 \times 10^{-4}$].

reported in a preliminary publication.[23] This slow mode, which we believe to be due to self-association of the hydroxyl groups, represents transient aggregates that eventually dissolve (over a period of months). The data shown in Figure 6a are limited to $w \leq 1.6 \times 10^{-2}$. In these solutions, the free-chain diffusion accounted for 80–100% of the DLS signal. We attribute the rest of the signal to artifacts such as dust and other difficulties due to the low scattering intensities from the THF solutions. However, the slow mode in the most concentrated solution ($w = 3.8 \times 10^{-2}$) persisted for 6 months and was detected consistently at all scattering angles. The main purpose of performing the DLS experiments on THF solutions was to obtain the R_h of the free chains. Hence, the $w = 3.8 \times 10^{-2}$ data were not used in this study. Whether equilibrium aggregates occur in THF solutions at $w > 1.6 \times 10^{-2}$ remains unresolved.

In Figure 6b we show the dependence of Γ_c of the PS–PSOH/toluene solutions on concentration and q^2. This relaxation mode is also diffusive and nearly independent of polymer concentration. The diffusion coefficient associated with these solutions is 5.18×10^{-8} cm²/s, with a corresponding $R_h = 76.4 \pm 2.6$ nm. This value is considerably larger than the size of the free chains and is evidence for micelle formation. This is expected because toluene is a selective solvent for the PS block. However, the fully extended length of the PS–PSOH molecule is 24 nm. The fact that the measured R_h in toluene is significantly greater than 24 nm rules out the possibility of spherical micelles with architecture depicted in Figure 1a. We therefore consider other possible structures such as cylindrical micelles.

Table 1. Dimensions of Ellipsoidal Particles Which, Based on Perrin's Theory,[25,26] Yield a Hydrodynamic Radius of 76.4 nm

minor semiaxes (nm)	major semiaxes (nm)		radius of sphere (nm)
	prolate	oblate	
4	405	117	
10	326	114	
15	275	112	
20	253	109	
25	220	104	
			76.4

The theory of scattering from ellipsoids was used to determine the structure of the micelles. A similar approach was used to determine the structure of biological macromolecules.[24] The rodlike and disklike micelles shown in Figure 1 may be approximated as prolate and oblate ellipsoids, respectively. The hydrodynamic radius of ellipsoids obtained by revolving an ellipse with semiaxes a and b about the a axis was obtained by Perrin.[19,24–26]

$$R_h = a/f(b/a) \tag{3}$$

where

$$f(b/a) = \frac{\ln\left[\dfrac{1 + (1 - b^2/a^2)^{1/2}}{b/a}\right]}{(1 - b^2/a^2)^{1/2}} \qquad \text{for } a > b \text{ (prolate)} \tag{4}$$

and

$$f(b/a) = \frac{\tan^{-1}[(b^2/a^2 - 1)^{1/2}]}{(b^2/a^2 - 1)^{1/2}} \qquad \text{for } a < b \text{ (oblate)} \tag{5}$$

For micellar aggregates, the minor semiaxis is restricted to molecular dimensions (see Figure 1). The lower and upper bounds for the minor semiaxes are thus 4 nm (the size of the free chains) and 25 nm (the fully extended chain length), respectively. It is well-known that block copolymer chains in micellar aggregates adopt stretched configurations, due to their proximity to each other.[1,4] Theoretical calculations and experimental observations on spherical micelles formed by block copolymers indicate that the radius of a micelle is about 4–5 times larger than the radius of gyration of the free chains.[3,4,27] The exact degree of stretching depends on the geometry and aggregation number. Since we do not know this for the PS–PSOH micelles, we assume that the degree of stretching is similar to that obtained in spherical micelles. The minor semiaxes of the micelles are thus expected to lie between 15 and 20 nm.

The major semiaxes of oblate and prolate ellipsoids that would obtain an R_h of 76.4 nm were computed from eqs 2–5, constraining the minor semiaxes to molecular dimensions. The results obtained are summarized in Table 1. For completeness, we also include the degenerate result that is obtained for a sphere ($b/a = 1$). We use SLS data to determine which of these structures is realized in toluene solutions of PS–PSOH.

The static scattering function, $I(q)$, of a solution containing randomly distributed ellipsoids is also well-known.[28]

$$I(q) = \frac{9\pi}{2}\int_0^{\pi/2} \frac{[J_{3/2}(u)]^2}{u^3} \cos\beta \, d\beta \tag{6}$$

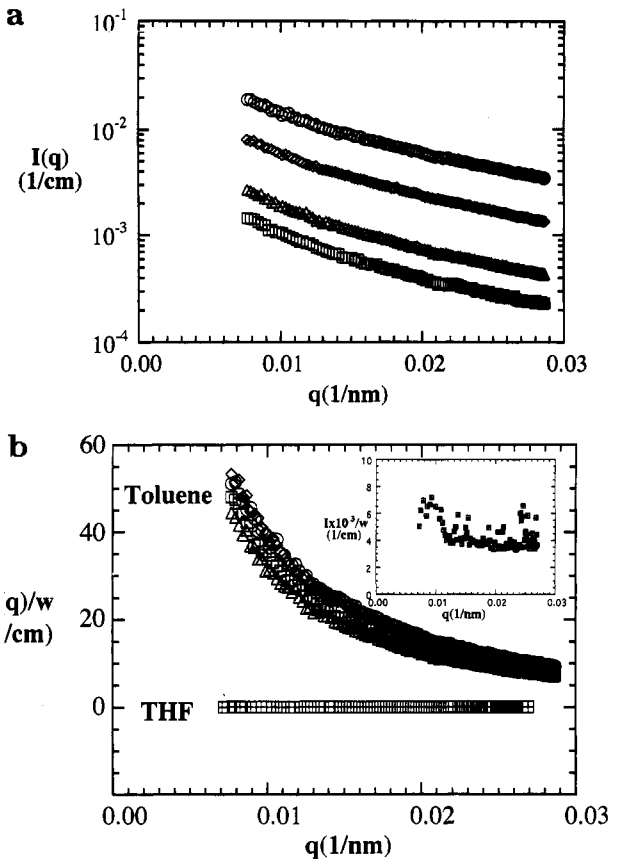

Figure 7. (a) SLS intensity, $I(q)$, versus q for PS–PSOH/toluene solutions at various concentrations [squares, $w = 6.0 \times 10^{-5}$; triangles, $w = 3.0 \times 10^{-5}$; diamonds, $w = 1.5 \times 10^{-4}$; circles; $w = 3.7 \times 10^{-4}$]. (b) Scattered intensity normalized by the weight fraction of polymer in solution, $I(q)/w$, versus q of PS–PSOH solutions in toluene [squares, $w = 6.0 \times 10^{-5}$; triangles, $w = 3.0 \times 10^{-5}$; diamonds, $w = 1.5 \times 10^{-4}$; circles, $w = 3.7 \times 10^{-4}$] and THF [hatched squares, $w = 1.3 \times 10^{-2}$]. Inset: THF scattering data shown in detail. The normalized scattered intensity from the toluene solutions is 4 orders of magnitude larger than that from the THF solutions.

where

$$u = qa\left(\cos^2\beta + \frac{b^2}{a^2}\sin^2\beta\right)^{1/2} \tag{7}$$

and $J_{3/2}(u)$ is the $^3/_2$-order Bessel function:

$$J_{3/2}(u) = \left(\frac{2u}{\pi}\right)^{1/2}\left(\frac{\sin u}{u^2} - \frac{\cos u}{u}\right) \tag{8}$$

In Figure 7a we show the absolute scattered intensity, $I(q)$, versus q from toluene solutions of PS–PSOH. In Figure 7b we plot the ratio $I(q)/w$ versus q and find that the data from all the solutions collapse on to a single curve. This collapse indicates that the size and shape of the aggregates do not change with concentration. This is consistent with the DLS results. For purposes of comparison, we also report absolute $I(q)/w$ values obtained from a typical THF solution ($w = 1.3 \times 10^{-2}$). Note that the normalized scattered intensity from the toluene solutions is 4 orders of magnitude larger than that obtained from the THF solutions. This suggests that the number of chains per aggregate is of the order of 10^4 (neglecting small differences such as scattering contrast in the two solutions). Conventional, spherical micelles formed by block copolymers usually contain 10^2 chains per aggregate.[3,4,27] The large aggregation number is thus also consistent with extended, nonspherical aggregates.

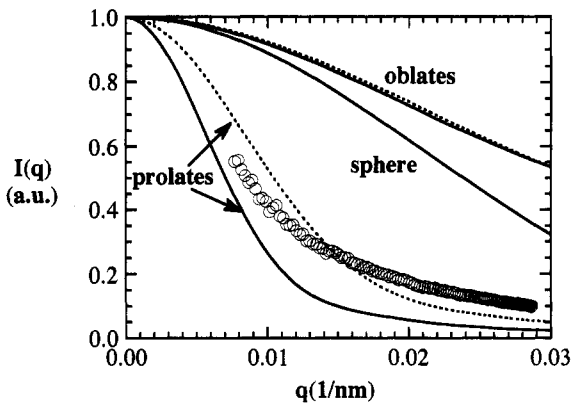

Figure 8. Comparison between experimentally measured SLS data and theoretical calculations for ellipsoids that give R_h = 76.4 nm (see Table 1). Prolate ellipsoids, i.e., rodlike particles, are most consistent with the experimental data. Solid curves: oblate ellipsoids with $a = 25$ nm and $b = 104$ nm, spheres with $a = b = 76.4$ nm, and prolate ellipsoids with $a = 326$ nm and $b = 10$ nm. Dashed curves: oblate ellipsoids with $a = 10$ nm and $b = 114$ nm and prolate ellipsoids with $a = 220$ nm and $b = 25$ nm. Symbols represent data obtained from the PS–PSOH/toluene solution with $w = 3.7 \times 10^{-4}$.

It is our purpose to determine which of the proposed micellar structures listed in Table 1 is most consistent with the measured $I(q)$. The q-dependence of the scattered intensity from the ellipsoidal structures listed in Table 1 was computed from eqs 6–8. The results are shown in Figure 8 along with data obtained from one of the PS–PSOH/toluene solutions. The experimental data were multiplied by a constant to force agreement between theory and experiment at the low scattering angles. We find qualitative consistency between experiment and theory for the case of prolate ellipsoids. On the other hand, spherical and disklike micelles are qualitatively inconsistent with the data. Note that spherical micelles could also be ruled out on the basis of the fully extended length of the PS–PSOH molecules. Prolate ellipsoids, i.e., rodlike structures, are thus the only structures that are consistent with *both* the static and dynamic light scattering data. We thus conclude that the micelles are most probably rodlike with length $L \approx 500$ nm and diameter $d \approx 40$ nm.

A more detailed description of the Brownian motion of rigid rods was obtained by Broersma.[29–31] According to this theory, the hydrodynamic radius of these particles is given by:

$$R_h = \frac{L}{2[\delta - g(\delta)]} \tag{9}$$

where $\delta = \ln(2L/d)$ and function $g(\delta)$ is given by

$$g(\delta) = 0.73 - 3.7(1/\delta - 0.34)^2 - 2.1(1/\delta - 0.39)^2 \tag{10}$$

In the limit $L/d \gg 1$, eqs 9 and 10 reduce to Perrin's results for long, prolate ellipsoids (eqs 3 and 4 with $b/a \ll 1$) and Reisman and Kirkwood's results[32] for rigid rods. Using Broersma's results with $R_h = 76.4$ nm and $d = 40$ nm, we obtain $L \approx 300$ nm. The agreement between theoretical $I(q)$ for these cylinders and experiment is qualitatively similar to that shown in Figure 8.

It is important to note that the actual micellar structure is far more intricate than the models that have been considered. The lack of quantitative agreement between theory and experiment seen in Figure 8 is

perhaps a manifestation of this fact. We have assumed that the micelles can be approximated as uniform, rigid bodies. The micelle, however, is a composite structure with a core that is much more rigid than the corona. The rigidity of the core will depend on the extent to which solvent is excluded from it. It is unlikely that cylindrical micelles with $L/d \approx 8$ are truly rigid. Furthermore, eqs 3–5, 9, and 10 were derived assuming the no-slip boundary condition; the velocity is assumed to be a continuous function across the fluid–particle interface. This is sometimes referred to as the "stick" boundary condition. This assumption may not be strictly valid due to the presence of mobile coronal chains at the particle–solvent interface. Additional effects, such as polydispersity in aggregate size, have not been considered. These factors may have a substantial effect on our estimate of L.[19,33,34] There is also some concern that the measured dynamic light scattering signal from such large micelles may contain contributions due to rotation of the cylinders.[19] Such effects are predicted to be important at high scattering angles ($qL > 6$). If our estimate of L (300 nm) were exact, then only DLS data obtained at scattering angles below 90° ($q < 6/L$) would yield the "true" translational diffusional coefficient. Departures from the Γ_c versus q^2 scaling are predicted at larger scattering angles ($q > 6/L$).[19] The fact that we do not observe such effects (see Figure 6b) suggests that the physical dimensions of the micelles may be somewhat smaller than that estimated on the basis of rigid, sticky cylinders.

Concluding Remarks

A nearly monodisperse polystyrene-*block*-poly(*p*-hydroxystyrene) block copolymer was synthesized using anionic polymerization techniques. We have used this model polymer to study the effect of hydrogen bonding on micelle formation in block copolymers. The characteristics of the micelles were studied by static and dynamic light scattering. The theory of scattering from ellipsoids was used to determine the shape of the aggregate. A cylindrical micelle with length $L \approx 300$ nm and diameter $d \approx 40$ nm is consistent with both static and dynamic light scattering measurements. Our current experiments are aimed at obtaining the structure of the micelle by other means such as electron microscopy. These studies may reveal other aspects of the micellar structure such as polydispersity.

Another factor that motivated this study is the "compatibilizing" capability of block copolymers.[35] In many systems, such as high-impact polystyrene, the addition of block copolymers to blends of immiscible polymers leads to improved properties. The copolymers serve as interfacial agents (or compatibilizers), improving the adhesion between the coexisting phases and preventing coalescence of the dispersed phase. We believe that it is possible to use molecules such as PS–PSOH to improve the properties of blends containing polymers with hydroxyl groups and other hydrogen-bonding groups such as ethers, amides, and esters.

Acknowledgment. We gratefully acknowledge the National Science Foundation for financial support. The work of J.Q.Z., E.M.P. and T.K.K. was supported by Grant No. DMR-9302375. The work of H.S.J., P.K.K., and N.P.B. was supported by Grant Nos. CTS-9308164 and DMR-9307098 and the NSF Young Investigator Program, Grant No. DMR-9457950. The synthesis of PS–PSOH would not have been possible without suggestions from Lew Fetters. We thank Jack Douglas, Bruce Garetz, and Tim Lodge for useful discussions.

References and Notes

(1) de Gennes, P.-G. *Solid State Phys., Suppl.* **1978**, *14*, 1.
(2) Bates, F. S.; Fredrickson, G. H. *Annu. Rev. Phys. Chem.* **1990**, *41*, 525.
(3) Tuzar, Z.; Kratochvil, P. *Adv. Colloid Interface Sci.* **1976**, *6*, 201.
(4) Leibler, L.; Orland, H.; Wheeler, J. C. *J. Chem. Phys.* **1983**, *79*, 3550.
(5) Chandrasekhar, S. *Liquid Crystals*, 2nd ed.; Cambridge University Press: Cambridge, Great Britain, 1992.
(6) de Gennes, P.-G.; Prost, J. *The Physics of Liquid Crystals*, 2nd ed.; Oxford University Press: New York, 1993.
(7) Forrest, B. J.; Reeves, L. W. *Chem. Rev.* **1981**, *81*, 1.
(8) Russel, W. B.; Saville, D. A.; Schowalter, W. R. *Colloidal Dispersions*; Cambridge University Press: New York, 1991.
(9) Price, C. *Pure Appl. Chem.* **1983**, *55*, 1563.
(10) Kinning, D. J.; Winey, K. I.; Thomas, E. L. *Macromolecules* **1988**, *21*, 3502.
(11) Nguyen, D.; Williams, C. E.; Eisenberg, A. *Macromolecules* **1994**, *27*, 5090.
(12) Desjardins, A.; Eisenberg, A. *Macromolecules* **1991**, *24*, 5779.
(13) Zhu, J.; Eisenberg, A.; Lennox, R. B. *J. Am. Chem. Soc.* **1991**, *113*, 5583.
(14) Bovey, F. A.; Winslow, F. H. In *Macromolecules: An Introduction to Polymer Science*; Academic Press: New York, 1979; Chapters 1 and 8.
(15) Pearce, E. M.; Kwei, T. K.; Min, B. Y. *J. Macromol. Sci., Chem.* **1984**, *A21*, 1181.
(16) Moskala, E. J.; Howe, S. E.; Painter, P. C.; Coleman, M. M. *Macromolecules* **1984**, *17*, 1671.
(17) Ishizone, T.; Hirao, A.; Nakahama, S. *Macromolecules* **1993**, *26*, 6964 and references therein.
(18) Morton, M.; Fetters, L. J. *Rubber. Chem. Technol.* **1975**, *48*, 359.
(19) Berne, B. J.; Pecora, R. *Dynamic Light Scattering*; Wiley: New York, 1976.
(20) Chu, B. *Laser Light Scattering*; Academic Press: New York, 1991.
(21) Provencher, S. *Makromol. Chem.* **1979**, *180*, 201.
(22) Huber, K.; Bantle, S.; Lutz, P.; Burchard, W. *Macromolecules* **1985**, *18*, 1461.
(23) Zhao, J. Q.; Pearce, E. M.; Kwei, T. K.; Kesani, P. K.; Jeon, H. S.; Balsara, N. P. *Proc. ACS, PMSE Div.* **1994** (Fall), *71*, 571.
(24) Dubin, S. B.; Clark, N. A.; Benedek, G. B. *J. Chem. Phys.* **1971**, *54*, 5158.
(25) Perrin, F. *J. Phys. Rad.* **1934**, *5*, 497.
(26) Perrin, F. *J. Phys. Rad.* **1936**, *7*, 1.
(27) Balsara, N. P.; Tirrell, M.; Lodge, T. P. *Macromolecules* **1991**, *24*, 1975.
(28) Kerker, M. *The Scattering of Light*; Academic Press: New York, 1969.
(29) Broersma, S. *J. Chem. Phys.* **1960**, *32*, 1626.
(30) Broersma, S. *J. Chem. Phys.* **1960**, *32*, 1632.
(31) Newman, J.; Swinney, H. L.; Day, L. A. *J. Mol. Biol.* **1977**, *116*, 593.
(32) Reisman, J.; Kirkwood, J. G. *J. Chem. Phys.* **1950**, *18*, 512.
(33) Douglas, J. F.; Zhou, H. X.; Hubbard, J. B. *Phys. Rev. E* **1994**, *49*, 5319.
(34) Hu, C.; Zwanzig, R. *J. Chem. Phys.* **1974**, *60*, 4354.
(35) Roe, R. J.; Rigby, D. *Adv. Polym. Sci.* **1987**, *82*, 103.

MA945021Q